Submitted to JPCC., 02/8/2024, revised 3/29/2024, revised again 4/30/2024

Multidimensional dynamics of CO_2 dissociative chemisorption on Cu(110)

Rongrong Yin and Hua Guo*

Department of Chemistry and Chemical Biology, Center for Computational Chemistry,

University of New Mexico, Albuquerque, NM 87131, USA

*: corresponding author: hguo@unm.edu

Abstract

In order to understand the recent experimentally measured initial sticking probability CO_2 on Cu(110), a globally accurate high-dimensional potential energy surface (PES) is constructed based on machine learning of density functional theory data. The reaction path revealed two saddle points flanking a chemisorbed CO_2 with a bent configuration, which serves as a precursor for dissociation. Quasi-classical trajectory studies on this PES found a small and monotonically increasing initial sticking probability, consistent with the recent experiment. The dissociation is enhanced by both incidence energy and internal excitation of the impinging CO_2. Mechanistic analysis revealed that the reaction is indirect and involves two very different reaction coordinates for the two barriers. The multi-dimensionality of the reaction path suggests that the one-dimensional model commonly used to describe direct dissociation is inadequate for this indirect process.

I. Introduction

Dissociative chemisorption is the initial and often rate-limiting step of many heterogeneous catalytic processes. Consequently, there have been extensive investigations of this process in recent years, from both experimental and theoretical perspectives.[1-6] The measured initial sticking probability often exhibits a S-shaped dependence on the incidence energy, starting with 0 and ending up at 1, which can be attributed to a single activation barrier along a "one-dimensional" reaction coordinate.[7] By fitting the S-shaped curve, one can in principle extract the effective barrier for a direct dissociative chemisorption process, which is near the midpoint of the S-shaped curve (~0.5). This approach has been quite successful for dissociation of several prototypical molecules, such as H_2,[8] CH_4,[9] and H_2O.[10]

The ever-increasing atmospheric CO_2 concentration due to consumption of fossil fuels has raised significant alarm for catastrophic climate changes due to greenhouse effect.[11] There have thus been extensive discussions on CO_2 conversion to value-added chemicals towards carbon neutrality, in which the activation of the stable greenhouse gas molecule constitutes the most challenging step.[12, 13] Recently, Singh and Shirhatti investigated the dissociative chemisorption of CO_2 on Cu(110),[14] which is considered as a model system for the activation of the greenhouse gas using, for example, reverse water-gas shift reaction.[15] The measured initial sticking probability is very small (~10^{-2}) and increases monotonically up to 1.5 eV of incidence energy. Fitting of the experimental dissociative probabilities to various S-shaped curves led the authors to conclude that the barrier is more than 2.0 eV. However, this conclusion is in sharp contrast to the calculated barrier of ~0.6 eV using density functional theory (DFT),[16, 17] which is in turn consistent with other experimental results.[18, 19]

In this work, we attempt to resolve this controversy by demonstrating that the dissociative chemisorption of CO_2 on Cu(110) is intrinsically multi-dimensional and indirect, similar to the same process on other metal surfaces.[20-23] These insights were provided by dynamical calculations on a high dimensional potential energy surface (PES), machine learned from DFT data for a CO_2 + Cu(110) model. The calculated dissociation probabilities are in semi-quantitative agreement with the measurement, but the dynamics revealed a more complex paradigm than the conventional one-dimensional single barrier picture. In particular, the dissociative pathway possesses two transition states, which flank a bent chemisorbed CO_2. Since the second barrier is much higher than the first, the majority of the incident CO_2 is scattered back to the gas phase while only a small portion undergoes bond cleavage. As a result, the one-dimensional model that has been successfully applied to direct dissociation processes is inadequate for describing this indirect dissociation process. This observation reenforces the emerging realization that dynamics play an key role in many surface processes.[4, 5, 24, 25] These dynamical calculations on this PES further revealed that the dissociation is enhanced by both the incidence energy and vibrational excitation in the impinging CO_2. These mode specificities are interpreted using the Sudden Vector Projection model.[26] Our theoretical insights help to gain deeper understanding of this important process, underscoring the importance of dynamics in surface processes.

II. Methods

IIA. Density Functional Theory and Data Sampling

The spin-unpolarized density functional theory (DFT) calculations were carried out using the Vienna Ab initio Simulation Package (VASP).[27, 28] The van der Waals interaction was taken

into account in all calculations by employing the optPBE-vdw functional[29] in order to better reproduce the experimental adsorption energy of CO_2 on Cu(110) surface.[30] The Kohn-Sham orbitals were expanded in terms of plane waves with an energy cutoff of 400 eV, while the projector augmented wave (PAW) method[31] was used to treat the core electrons. The dipole correction in the *Z* direction was imposed to avoid artificial interaction between the vertically repeated images. Fermi smearing with a width parameter of 0.1 eV was used. These geometries were optimized using a conjugate-gradient method until the forces acting on each atom were less than 0.02 eV/Å. The saddle points were determined using the climbing image nudged elastic band (CI-NEB)[32] and dimer methods,[33] and confirmed by frequency calculations. The calculated lattice constant for bulk Cu is 3.646 Å, in good agreement with the experimental value 3.615 Å.[34]

The Cu(110) surface was modeled by a six-layer slab with a (3×3) supercell with the top three layers relaxed. The slabs were separated by a 20 Å vacuum space to avoid interslab interaction. The first Brillouin zone was sampled with a (4×6×1) Monkhorst-Pack *k*-point mesh.[35] The convergence of the adsorption energies and barrier heights were confirmed with respect to the *k*-point mesh, energy cutoff, slab layers, and the supercells. The adsorption energy was computed as follows: $E_{adsorbate@slab} - E_{adsorbate} - E_{slab}$, where $E_{adsorbate@slab}$, $E_{adsorbate}$, E_{slab}, are the energies of the adsorbed system, the gas-phase molecule, and the bare surface, respectively.

To construct the high-dimensional PES for the CO_2 + Cu(110) system, ab initio molecular dynamics (AIMD) simulations of the surface scattering and dissociation processes were performed to sample the configuration space. The initial surface configurations were taken from equilibrated canonical (NVT) AIMD snapshots of the clean surface at surface temperature

T_s=300 K. Microcanonical AIMD trajectories were then initiated with CO_2 being 6.0 Å above the Cu(110) surface with incidence energies E_i = 1.7 and 2.0 eV and velocity pointing towards the surface along the surface normal. The initial lateral positions within the surface supercell and orientations of the CO_2 molecule were sampled randomly, with zero rotational angular momentum. The atomic cartesian coordinates and momenta of CO_2 are sampled from the normal modes. Some of the simulations involve CO_2 molecules with different normal mode quantum numbers (v_{ss}, v_b, v_{as}). These AIMD trajectories were propagated using the leapfrog algorithm in VASP with a time step of 1.0 fs, up to a maximum propagation time of 10 ps.

We first selected 4599 points out of 30816 points from 150 AIMD trajectories, according to their generalized Euclidian distances (GEDs) in terms of inter-nuclear distances.[36] These initial data set was used to train a preliminary PES, using a machine learning method described below. This preliminary PES enabled QCT calculations for vibrationally excited CO_2 molecules impinging at the Cu(110) surface. New data points from these trajectories were selectively included into the training set based on the same GED criterion so that they were not too close to existing points. The augmented data set was then used to update the PES, followed by a new iteration of QCT calculations. This process was repeated until the dissociative sticking probabilities of CO_2 were converged.

IIB. Neural Network Potential Energy Surface

Although AIMD represents a robust method for investigating chemical dynamics, it is computationally expensive owing to the repeated DFT calculations along trajectories. The situation is particularly unfavorable for rare and prolonged events. A recent advance involves replacing the on-the-fly DFT calculations with a machine-learned high-dimensional PES.[37, 38]

Such PESs are necessarily high-dimensional because a large number of surface atoms have to be included to account for the energy transfer accompanying the collision process.[24] In this work, the CO_2 + Cu(110) PES was constructed by means of the embedded atom neural network (EANN) approach.[39] In the EANN framework, the total energy of the system is a sum of atomic energies, each of which is an output of an atomic NN determined by its environment consisting of other atoms nearby,[39]

$$E = \sum_{i=1}^{N} E_i = \sum_{i=1}^{N} NN_i\left(\boldsymbol{\rho}^i\right). \tag{1}$$

For simplicity, the density-like structural descriptors ($\boldsymbol{\rho}^i$) can be represented by Gaussian-type orbitals (GTOs) centered at neighboring atoms, resulting in multiple orbital-dependent components,

$$\rho^i_{L,\alpha,r_s} = \sum_{l_x,l_y,l_z}^{l_x+l_y+l_z=L} \frac{L!}{l_x!l_y!l_z!}\left(\sum_{j=1}^{n_{atom}} c_j \varphi^{\alpha,r_s}_{l_x,l_y,l_z}\left(\mathbf{r}_{ij}\right) f_c(r_{ij})\right)^2, \tag{2}$$

where n_{atom} is the total number of atoms lying nearby the embedded atom within a cutoff radius (r_c) and $f_c(r_{ij})$ a cutoff function[40] to ensure that the contribution of each neighbor atom decays smoothly to zero at r_c. The GTO is written as,

$$\varphi^{\alpha,r_s}_{l_x,l_y,l_z}\left(\mathbf{r}_{ij}\right) = x^{l_x} y^{l_y} z^{l_z} \exp\left(-\alpha\left|r_{ij} - r_s\right|^2\right), \tag{3}$$

where r_{ij} is the distance between atoms i and j, l_x, l_y and l_z represent the angular momentum components in each axis, and their sum is the total orbital angular momentum (L), α and r_s are parameters that determine radial distributions of GTOs. Note that c_j in Eq. (2) serve as element-dependent expansion coefficients of an atomic orbital for atom j, which is optimized together with the element-dependent NN parameters. The EANN PES is invariant with respect to

translation, rotation, and permutation.[39] The key advantage of this EANN method is that the density-like descriptors given in Eq. (2) scale linearly with the number of neighboring atoms.[41]

IIC. Classical Trajectory Calculations

QCT calculations were performed with the VENUS code[42] which is modified for surface dynamics calculations.[43] As in the AIMD calculations, the initial surface configurations were sampled randomly from a NVT run of the surface at the target surface temperature T_s=300 K. The initial CO_2 molecule was launched from 7.0 Å above the Cu(110) surface, whose orientation and position in the surface supercell were sampled randomly. To compare with experiment,[14] the CO_2 molecule was launched towards the surface along the surface normal with the initial translational energy ranging from 0.5 to 2.0 eV. In our QCT calculations, the CO_2 molecule is assumed to be rotationless. Several different initial vibrational states of CO_2 were prepared to explore the mode specificity and the corresponding atomic coordinates and momenta were sampled with the standard normal mode sampling scheme. These vibrational states are denoted by three normal mode quantum numbers (v_{ss}, v_b, v_{as}) for the symmetric stretching, (doubly degenerate) bending, and asymmetric stretching modes. Each trajectory was propagated via the velocity Verlet algorithm in QCT with a time step of 0.1 fs, up to a maximum propagation time of 10 ps. The trajectory was terminated and labeled as "reactive" when one of the C−O bond lengths became larger than 3.0 Å, or "scattered" when the molecule was flying away from the surface by 6.9 Å. Otherwise, the trajectory was labeled as "trapped" and terminated after 10 ps.

III. Results

IIIA. Potential Energy Surface

Firstly, we assess the properties of the CO_2 + Cu(110) PES. The final PES was trained with 11488 DFT points, which include both energies and forces. These data points were divided into training and test sets with the ratio of 90:10. The hyperparameters of GTOs were L=0, 1, 2, r_c=6.8 Å, α=0.46 Å^{-2}, and Δr_s=0.658 Å, resulting in 33 structural parameters. Each atomic NN consists of two hidden layers with 50 and 60 neurons in each. The Root Mean Squared Errors (RMSEs) for total energies and atomic forces in both the training and validation sets are 9.40/16.40 meV and 14.43/19.72 meV/Å, respectively.

To demonstrate the quality of the EANN fitting, we compare the energies and geometries of stationary points along the minimum energy path (MEP) for the CO_2 dissociative chemisorption process on the Cu(110) surface, optimized with both DFT and EANN PES. The EANN PES reproduces the barrier energies, adsorption well depths, and reaction energy with a deviation of only 33 meV. Additionally, the EANN PES accurately replicates the geometries of stationary points (with a maximum deviation of 0.06 Å), as illustrated in Figure 1.

Generally, CO_2 adsorption on transition metal surfaces exhibits both physi- and chemi-sorption configurations.[44-47] The Cu(110) surface is no exception. However, different from the CO_2 adsorption on the Ni(100)[20] or W(110) surface,[23] the physiosorbed CO_2 is more stable than chemisorbed CO_2 on the Cu surface. The physiosorbed CO_2 on Cu(110) features a linear configuration, with an adsorption energy of -0.24 eV, which is consistent with the experimental result, -0.22 eV.[30] At the chemisorbed state, a bent-CO_2* featuring a $\angle$OCO angle of 126.0º with elongation of both C-O bonds to 1.275 Å. It is metastable relative to the gas phase CO_2 by 0.064 eV, consistent with the experimental failure in observing this species.[48] The bent-CO_2* adsorbate adopts a tridentate configuration, with two oxygen and carbon bonded with Cu

atoms, as illustrated in Figure 1. There is a saddle point (TS1) that connects the physisorbed linear-CO_2* to the chemisorbed bent-CO_2* with a forward barrier of 0.38 eV. The CO_2 moiety at TS1 is slightly bent (∠OCO=148.1°), as expected.

The chemisorbed CO_2* is a precursor for dissociation, which has a dissociation barrier (TS2) of 0.57 eV. The transition state features the elongation of the OC-O bond (1.862 Å) and a smaller ∠OCO angle (112.8°), accompanied with the formation of CO* and O* adsorbates near two short bridge (SB) sites. TS2 represents a "late" barrier, as shown in Figure 1. In the product side, which is ~0.4 eV above the reactant asymptote, the CO* adsorbed at the top site nearly perpendicular to the surface plane, while O* resides near the SB sites. The maximal displacement of Cu atoms in the top two layers along the surface normal is found to be 0.008 Å, 0.068 Å, 0.106 Å, -0.087 Å, and 0.111 Å, respectively, for the linear-CO_2*, TS1, bent-CO_2*, TS2, and CO*+O* configurations, which imply that surface temperature may exert an influence on the dissociation process.

Figure 2 displays several cuts of the PES as a function of the COM distance of the CO_2 from the surface (Z) and the rupturing OC-O bond (d_{O1C-O2}). In each panel, the other geometric parameters were fixed at key stationary points, and geometries of the saddle points are superimposed on the contours. These plots provide different perspectives of the high-dimensional topography of the reaction path, although they do not always pass through the MEP shown in Figure 1. It is clear that the PES is smooth and free of artifacts.

IIIB. Scattering and Dissociation Dynamics

With the PES, we performed extensive dynamical calculations for CO_2 colliding with the Cu(110) surface using the QCT method. Over 5000 trajectories were calculated at each

incidence energy to achieve satisfactory statistics. We will focus on chemisorption, and neglect the low-energy trapping in the physisorption well.[49] In Figure 3, we compared the dissociative sticking probabilities (S_0) of CO_2 at normal incidence with the recent molecular beam experiment at the nozzle temperature (T_N) of 300 K. Two theoretical curves are presented, and they are quite similar, due to the fact that the Boltzmann populations of the vibrationally excited states are quite small. The first is for the ground ro-vibrational state of CO_2, while the other is for 300 K of vibrational temperature, which was obtained from vibrational state specific sticking probabilities presented below. It is clear that our QCT results qualitatively reproduce the magnitude of the experimental S_0 ($\sim 10^{-2}$) and its dependence on the incidence energy. Quantitatively, however, the theoretical values systematically underestimate the corresponding experimental probabilities.

To investigate the impact of vibrational excitation of CO_2 on dissociation, we further carried out initial state-specific QCT calculations in which the CO_2 is sampled with different excitations in its normal modes. In Figure 4a, these calculated dissociative sticking probabilities (S_0) for several CO_2 vibrational states at normal incidence are displayed as a functional of incidence translational energy. From the figure, it is clear that the reactivity is enhanced by excitation of any given CO_2 vibrational mode, symmetric stretch (v_{ss}), antisymmetric stretch (v_{as}) or bend (v_b). The confirmation of the mode specificity has to await experimental confirmation with vibrational state specific preparation of the incident CO_2. It is worth mentioning that there are two degenerate bending modes in this linear molecule, but in our approximate treatment, they are considered as an effective single mode. In other words, v_b = 1 and 2 correspond to one and two quanta in these modes.

To properly assess the vibrational efficacies of various molecular modes, one needs to compare the reactivity in terms of the total energy. Here, the total energy is defined as the sum of translational and internal energies. From Figure 4(b), we can find that all vibrational excitations are more effective in promoting the dissociation than the translational excitation, with the antisymmetric stretch mode being the most effective. These data are used in generating the T_N=300 K result in Figure 3.

To understand the origin of the small sticking probabilities, the capture probabilities of CO_2 chemisorption over TS1 are computed as a function of the incidence energy and vibrational excitation. Here, the capture probability (C_0) is defined as the number of trajectories that pass over TS1 and enter the chemisorption well divided by the total number of trajectories. In Figure 4(c, d), it is evident that the C_0 is significantly larger than S_0, suggesting the impinging CO_2 can enter the chemisorption well with relative ease. Indeed, at 2.0 eV of incidence energy, nearly all (~85 %) of the trajectories visit the chemisorption well. However, only a tiny fraction (~1%) go on to dissociate. In total energy scale, the most effective promotional mode is the incidence energy, although internal excitations also help.

To shed light on the origin of the mode specificity observed in the CO_2 collisional process on Cu(110), we relied on the Sudden Vector Projection (SVP) model,[26] in which the projection of a reactant normal mode onto the reaction coordinate at the transition state is taken as its ability for promoting the reactivity. As shown in Table 1, the SVP values for TS1 suggest that the translational mode along the surface normal direction (*Z*) is the most effective. This explains the promotional effect of the incidence energy for both S_0 and C_0, as shown in Figure 4. The SVP values for TS2 are also listed in Table 1, which indicate that the three vibrational

modes are more impactful than the translational modes, with the antisymmetric stretch mode exhibiting the highest efficacy. This is consistent with the mode specificity for S_0 shown in Figure 4. These SVP values for both TS1 and TS2 suggest complicated reaction dynamics in which the CO_2 dissociative chemisorption process on Cu(110) is affected by both barriers and thus intrinsically multidimensional.

In order to gain further insight into the CO_2 dissociation dynamics on Cu(110), we calculated averaged characteristic times for the scattered and dissociative trajectories. These characteristic times T_{diss}, T_{scat}, T_{TS1}, $T_{TS1\text{-}TS2}$, are $T_{TS1\text{-}TS1}$ are defined as the time for CO_2 to dissociate, to scatter, to pass TS1, to stay between TS1 and TS2, and to make a round-trip to TS1. In Table 2, it is observed that CO_2 dissociative chemisorption and the non-reactive CO_2 scattering take approximately 654 (T_{diss}) and 1224 fs (T_{scat}), respectively. Both spend a significant time in the CO_2 chemisorption well, which is characterized by an averaged lifetime of ~400 fs ($T_{TS1\text{-}TS2}$) for dissociative and ~1000 fs ($T_{TS1\text{-}TS1}$) for scattered trajectories. The long lifetime suggests that a trapping-desorption (TD) mechanism for the scattering of CO_2 from the surface.

To explain these interesting observations, we plotted in Figure 5 the kinetic energies and geometries as a function of time for two exemplary trajectories for the impinging CO_2(v=0) with incidence translational energy of 1.7 eV. For the dissociative trajectory, the passing of TS1, which occurs roughly at 200 fs and characterized by the drastic reduction of the ∠OCO angle, transfer the translational energy of the impinging CO_2 to the surface phonons, evidenced by the increasing kinetic energy of the Cu surface atoms. However, the OC-O bond rupture does not happen until 600 fs, during which the bent CO_2 explores the chemisorption well in search of

TS2. For the scattered trajectory, on the other hand, the passing of TS1 occurs at about the same time (~200 fs), forming the chemisorbed CO_2*. After about 400 fs, the trapped CO_2* loses some energy to the Cu surface phonons, but managed to exit to the gas phase through TS1. As shown in Figure 1, TS2 is much higher in energy than TS1, which explains that the majority of the trapped CO_2 would desorb back to the gas phase, while only a small portion dissociate.

There is ample additional evidence for the transient trapping of CO_2 during the scattering, which can be experimentally measurable. In Figure 6, the angular and translational energy distributions of scattered CO_2 are plotted for T_{scat} smaller and larger than 2 ps, which we use to approximately characterize the TD and IS (impulsive scattering) mechanisms. For the incidence energy of 1.7 eV for ground state CO_2, the ratio of the two channels is about 10:90. It can be clearly seen that the IS trajectories have a narrow angular distribution along the surface normal and a translational energy distribution peaking near 0.3 eV. On the other hand, the TD trajectories feature a near $\cos(\theta)$ distribution with a monotonically decaying translational energy distribution, which is also much colder than the IS counterpart. The latter is apparently due to the energy dissipation in the chemisorbed well. Significant internal excitations are noted in the desorbed CO_2, but not quantified. We note also that there are still a small percentage (~4%) of trajectories that are trapped on the surface at the end of the propagation, but they are unlikely to impact the conclusion.

IV. Discussion

It is interesting to compare the current case with two other systems investigated theoretically before, namely CO_2 dissociation on Ni(100)[20] and W(110).[23] Although all three systems possess both physi- and chemi-sorption wells, their energetics are quite different. The

Ni(100) system has stable physi- and chemi-sorption wells with the two barriers (TS1 and TS2) at roughly the same low energy. On the other hand, the W(110) surface features a much deeper chemisorption well and a near-zero barrier for dissociation (TS2). On Cu(110), the chemisorption well is metastable and TS2 is significantly higher than TS1. These different topographies result in very different dissociation dynamics. On W(110), the dissociation after passing TS1 is almost complete, thanks to the low TS2 barrier. For Ni(100), on the other hand, dissociation is known to be inefficient,[50] even with low energy barriers. This is because the TS2, despite its low energy, is very tight and only a small fraction of trajectories manages to pass through.[20] The situation for Cu(110) is similar to Ni(100), as we discussed in this work, the TS2 barrier is quite high, leaving many impinging CO_2 scattered back to the gas phase. In both Ni and Cu cases, it is clear that the dynamics is multidimensional, involving both TS1 and TS2. The dissociation bottleneck is the TS2 barrier, which leads to small dissociative sticking probabilities.

In both Ni and Cu cases, the dissociation is promoted by incidence energy, evidenced by the increase of S_0 as a function of the incidence energy. This can be attributed to the fact that the formation of the chemisorption CO_2 intermediate is a necessity for dissociation. Our theoretical models for the two surfaces predict that vibrational excitations also have a significant impact on S_0. This is due apparently to TS2, according to the SVP analysis. Quantitatively, the vibrational efficacy depends on the rate of energy dissipation in the chemisorption well, which are significant on both Ni(100)[21] and Cu(111). For those trajectories that lose most of their energies, reaction becomes impossible due to the tight TS2 bottleneck, and they eventually desorb. Only those trajectories that have sufficient energy along the

reaction coordinate of TS2 are productive. The dependence of S_0 on the incident CO_2 vibrational excitation is a testament that the energy of the chemisorption CO_2 is not completely randomized, due apparently to the finite lifetime of this reaction intermediate.

These insights underscore the importance of the chemisorbed CO_2 species, which has a bent geometry due apparently to electron injection into the antibonding orbital of CO_2.[47] Such a bent species have been spectroscopically identified before on various transition metal surfaces.[51, 52] Dynamical signatures have also been found. Recently, for example, Wodtke and coworkers have observed two types of CO_2 desorbed from oxidation of CO* on Pt surfaces, with thermal and hyperthermal translational energy distributions.[53] Detailed theoretical studies have attributed the thermal channel to the transient trapping of chemisorbed CO_2 at steps of the Pt surface, which dissipates most of its energy gained from the transition state.[54] In the current system, we have also shown that the angular and translational energy distributions of scattered CO_2 contain signatures of the chemisorbed species. The existence of this reaction intermediate makes the CO_2 dissociative chemisorption on Cu(110) an indirect process.

The theoretical evidence presented in this work also clarifies the "curious" nature of the recent experimental observation by Singh and Shirhatti.[14] As discussed above, the barrier of direct dissociation process can in principle be extracted from the one-dimensional model, in which the sticking probability near the barrier is near 0.5. This model apparently led Singh and Shirhatti to conclude that the barrier for CO_2 dissociation on Cu(110) has to be much higher than the observed threshold for S_0 (~0.9 eV). The observed threshold and monotonically increase S_0 with incidence energy are reproduced by our theory, which features a barrier near 0.6 eV. It is thus quite clear that the underlying assumption of the S-shaped curve for S_0 is only

applicable to direct dissociation characterized by a single transition state, but not applicable for the multidimensional and indirect dissociation of CO_2. In other words, the experimentally observed small and monotonically increasing S_0 with incidence energy, which is successfully reproduced in this work, is not in conflict with the moderate barrier of ~0.6 eV predicted by DFT.

We note in passing that the theory-experiment agreement in Figure 3 is not quantitative, as the theoretical values are lower than the experimental counterparts. There might be multiple reasons for this discrepancy. First, the functional used in the DFT calculations might not be quantitatively accurate, which is a well-established fact. As a result, one does not generally expect that the DFT based PES to quantitatively reproduce the experimental data, particularly with such small S_0. Second, there might be experimental uncertainties as the error bars at higher energies are notably larger.

V. Conclusions

In this work, we report a globally accurate high-dimensional PES for the dissociative chemisorption of CO_2 on the Cu(110) surface using machine learning based on DFT data. Quasi-classical trajectory (QCT) studies on this PES demonstrate a small and monotonically increasing initial sticking probability with the incidence energy, reproducing the recent experimental observations.

The PES reveals a unique reaction path with two saddle points flanking a metastable chemisorbed CO_2 with a bent configuration, acting as a precursor for dissociation. The reactivity is primarily controlled by the second "late" barrier, TS2. Our QCT results emphasize that reactivity is enhanced not only by translational excitation but also by all CO_2 vibrational

modes, with the vibrationally antisymmetric stretching mode proving to be the most influential. Importantly, the chemisorbed CO_2 species has a significant lifetime, during which it loses it energy to surface phonons. This long-lived intermediate leads to both dissociation and scattering. The latter has two components with drastically different translational energy distributions, which correlate with the time spent in the chemisorption well.

These theoretical insights reveal that the reaction is indirect, involving at least two distinct reaction coordinates for the two barriers. This multidimensional nature of the reaction path challenges the adequacy of the commonly used one-dimensional model for describing direct dissociation.

Acknowledgements: This work is supported by the National Science Foundation (CHE-1951328 and CHE-2306975). The computations were performed at the Center for Advanced Research Computing (CARC) at UNM. We thank Prof. Pranav Shirhatti for several useful discussions and for sharing the experimental data.

References:

(1) Kroes, G.-J. Frontiers in surface scattering simulations. *Science* **2008**, *321*, 794-797.
(2) Juurlink, L. B. F.; Killelea, D. R.; Utz, A. L. State-resolve probes of methane dissociation dynamics. *Prog. Surf. Sci.* **2009**, *84*, 69-134.
(3) Chadwick, H.; Beck, R. D. Quantum state resolved gas-surface reaction dynamics experiments: A tutorial review. *Chem. Soc. Rev.* **2016**, *45*, 3576-3594.
(4) Luntz, A. C. Dynamics of Gas-Surface Interactions. In *Surface and Interface Sciences: Solid-Gas Interface II*, Wandelt, K. Ed.; Wiley-VCH Verlag, 2016.
(5) Jiang, B.; Yang, M.; Xie, D.; Guo, H. Quantum dynamics of polyatomic dissociative chemisorption on transition metal surfaces: Mode specificity and bond selectivity. *Chem. Soc. Rev.* **2016**, *45*, 3621-3640.
(6) Guo, H.; Farjamnia, A.; Jackson, B. Effects of lattice motion on dissociative chemisorption: Toward a rigorous comparison of theory with molecular beam experiments. *J. Phys. Chem. Lett.* **2016**, *7*, 4576-4584.
(7) Luntz, A. C. A simple model for associative desorption and dissociative chemisorption. *J. Chem. Phys.* **2000**, *113*, 6901-6905.

(8) Michelsen, H. A.; Rettner, C. T.; Auerbach, D. J.; Zare, R. N. Effect of rotation on the translational and vibrational energy dependence of the dissociative adsorption of D_2 on Cu(111). *J. Chem. Phys.* **1993**, *98*, 8294-8307.
(9) Smith, R. R.; Killelea, D. R.; DelSesto, D. F.; Utz, A. L. Preference for vibrational over translational energy in a gas-surface reaction. *Science* **2004**, *304*, 992-995.
(10) Hundt, P. M.; Jiang, B.; van Reijzen, M.; Guo, H.; Beck, R. D. Vibrationally promoted dissociation of water on Ni(111). *Science* **2014**, *344*, 504-507.
(11) Haszeldine, R. S. Carbon capture and storage: How green can black be? *Science* **2009**, *325*, 1647-1652.
(12) Arakawa, H.; Aresta, M.; Armor, J. N.; Barteau, M. A.; Beckman, E. J.; Bell, A. T.; Bercaw, J. E.; Creutz, C.; Dinjus, E.; Dixon, D. A.; et al. Catalysis research of relevance to carbon management: Progress, challenges, and opportunities. *Chem. Rev.* **2001**, *101*, 953-996.
(13) Khodakov, A. Y.; Chu, W.; Fongarland, P. Advances in the development of novel cobalt Fischer–Tropsch catalysts for synthesis of long-chain hydrocarbons and clean fuels. *Chem. Rev.* **2007**, *107*, 1692-1744.
(14) Singh, S. K.; Shirhatti, P. R. The curious case of CO_2 dissociation on Cu(110). *J. Chem. Phys.* **2024**, *160*, 024702.
(15) Dietz, L.; Piccinin, S.; Maestri, M. Mechanistic Insights into CO_2 activation via reverse water–gas shift on metal surfaces. *J. Phys. Chem. C* **2015**, *119*, 4959-4966.
(16) Muttaqien, F.; Hamamoto, Y.; Inagaki, K.; Morikawa, Y. Dissociative adsorption of CO_2 on flat, stepped, and kinked Cu surfaces. *J. Chem. Phys.* **2014**, *141*, 034702.
(17) Yang, T.; Gu, T.; Han, Y.; Wang, W.; Yu, Y.; Zang, Y.; Zhang, H.; Mao, B.; Li, Y.; Yang, B.; Liu, Z. Surface orientation and pressure dependence of CO_2 activation on Cu surfaces. *J. Phys. Chem. C* **2020**, *124*, 27511-27518.
(18) Nakamura, J.; Rodriguez, J. A.; Campbell, C. T. Does CO_2 dissociatively adsorb on Cu surfaces? *J. Phys. Condens. Matter* **1989**, *1*, SB149.
(19) Rasmussen, P. B.; Taylor, P. A.; Chorkendorff, I. The interaction of carbon dioxide with Cu(100). *Surf. Sci.* **1992**, *269–270*, 352-359.
(20) Jiang, B.; Guo, H. Communication: Enhanced dissociative chemisorption of CO_2 via vibrational excitation. *J. Chem. Phys.* **2016**, *144*, 091101.
(21) Zhou, X.; Kolb, B.; Luo, X.; Guo, H.; Jiang, B. Ab Initio molecular dynamics study of dissociative chemisorption and scattering of CO_2 on Ni(100): Reactivity, energy transfer, steering dynamics, and lattice effects. *J. Phys. Chem. C* **2017**, *121*, 5594-5602.
(22) Farjamnia, A.; Jackson, B. The dissociative chemisorption of CO_2 on Ni(100): A quantum dynamics study. *J. Chem. Phys.* **2017**, *146*, 074704.
(23) Yin, R.; Guo, H. Dynamics of CO_2 dissociative chemisorption on W(110). *J. Phys. Chem. C* **2022**, *126*, 17935-17941.
(24) Jiang, B.; Guo, H. Dynamics in reactions on metal surfaces: A theoretical perspective. *J. Chem. Phys.* **2019**, *150*, 180901.
(25) Muiño, R. D.; Busnengo, H. F. *Dynamics of Gas-Surface Interactions*; Springer, Heidelberg, 2013.
(26) Guo, H.; Jiang, B. The sudden vector projection model for reactivity: Mode specificity and bond selectivity made simple. *Acc. Chem. Res.* **2014**, *47*, 3679-3685.
(27) Kresse, G.; Furthmuller, J. Efficient iterative schemes for ab initio total-energy calculations using plane wave basis set. *Phys. Rev. B* **1996**, *54*, 11169-11186.
(28) Kresse, G.; Furthmuller, J. Efficiency of ab initio total energy calculations for metals and semiconductors

using plane wave basis set. *Comp. Mater. Sci.* **1996**, *6*, 15-50.
(29) Klimeš, J.; Bowler, D. R.; Michaelides, A. Chemical accuracy for the van der Waals density functional. *J. Phys.: Condens. Matter* **2010**, *22*, 022201.
(30) Ernst, K. H.; Schlatterbeck, D.; Christmann, K. Adsorption of carbon dioxide on Cu(110) and on hydrogen and oxygen covered Cu(110) surfaces. *Phys. Chem. Chem. Phys.* **1999**, *1*, 4105-4112.
(31) Blöchl, P. E. Projector augmented-wave method. *Phys. Rev. B* **1994**, *50*, 17953-17979.
(32) Henkelman, G.; Uberuaga, B. P.; Jónsson, H. A climbing image nudged elastic band method for finding saddle points and minimum energy paths. *J. Chem. Phys.* **2000**, *113*, 9901-9904.
(33) Henkelman, G.; Jónsson, H. A dimer method for finding saddle points on high dimensional potential surfaces using only first derivatives. *J. Chem. Phys.* **1999**, *111*, 7010-7022.
(34) Lattice parameters, densities, expansion coefficients and perfection of structure of Cu and of Cu–In α phase. http://hdl.handle.net/11256/34
(35) Monkhorst, H. J.; Pack, J. D. Special points for Brillouin-zone integrations. *Phys. Rev. B* **1976**, *13*, 5188-5192.
(36) Jiang, B.; Li, J.; Guo, H. Potential energy surfaces from high fidelity fitting of ab initio points: The permutation invariant polynomial-neural network approach. *Int. Rev. Phys. Chem.* **2016**, *35*, 479-506.
(37) Behler, J. Perspective: Machine learning potentials for atomistic simulations. *J. Chem. Phys.* **2016**, *145*, 170901.
(38) Jiang, B.; Li, J.; Guo, H. High-fidelity potential energy surfaces for gas phase and gas-surface scattering processes from machine learning. *J. Phys. Chem. Lett.* **2020**, *11*, 5120-5131.
(39) Zhang, Y.; Hu, C.; Jiang, B. Embedded atom neural network potentials: Efficient and accurate machine learning with a physically inspired representation. *J. Phys. Chem. Lett.* **2019**, *10*, 4962-4967.
(40) Behler, J. Atom-centered symmetry functions for constructing high-dimensional neural network potentials. *J. Chem. Phys.* **2011**, *134*, 074106.
(41) Zhou, X.; Zhang, Y.; Yin, R.; Hu, C.; Jiang, B. Neural network representations for studying gas-surface reaction dynamics: Beyond the Born-Oppenheimer static surface approximation. *Chin. J. Chem.* **2021**, *39*, 2917-2930.
(42) Hase, W. L.; Duchovic, R. J.; Hu, X.; Komornicki, A.; Lim, K. F.; Lu, D.-H.; Peslherbe, G. H.; Swamy, K. N.; Linde, S. R. V.; Varandas, A.; et al. VENUS96: A General Chemical Dynamics Computer Program. *Quantum Chemistry Program Exchange Bulletin* **1996**, *16*, 671.
(43) Jiang, B.; Guo, H. Dynamics of water dissociative chemisorption on Ni(111): Effects of impact sites and incident angles. *Phys. Rev. Lett.* **2015**, *114*, 166101.
(44) Wang, S.-G.; Liao, X.-Y.; Cao, D.-B.; Huo, C.-F.; Li, Y.-W.; Wang, J.; Jiao, H. Factors controlling the interaction of CO_2 with transition metal surfaces. *J. Phys. Chem. C* **2007**, *111*, 16934-16940.
(45) Liu, C.; Cundari, T. R.; Wilson, A. K. CO_2 reduction on transition metal (Fe, Co, Ni, and Cu) surfaces: In comparison with homogeneous catalysis. *J. Phys. Chem. C* **2012**, *116*, 5681-5688.
(46) Liu, X.; Sun, L.; Deng, W.-Q. Theoretical investigation of CO_2 adsorption and dissociation on low index surfaces of transition metals. *J. Phys. Chem. C* **2018**, *122*, 8306-8314.
(47) Jin, W.; Wang, Y.; Liu, T.; Ding, C.; Guo, H. CO_2 chemisorption and dissociation on flat and stepped transition metal surfaces. *Appl. Surf. Sci.* **2022**, *599*, 154024.
(48) Fu, S. S.; Somorjai, G. A. Interactions of O_2, CO, CO_2, and D_2 with the stepped Cu(311) crystal face: Comparison to Cu(110). *Surf. Sci.* **1992**, *262*, 68-76.
(49) Funk, S.; Hokkanen, B.; Wang, J.; Burghaus, U.; Bozzolo, G.; Garcés, J. E. Adsorption dynamics of CO_2 on Cu(110): A molecular beam study. *Surf. Sci.* **2006**, *600*, 583-590.

(50) D'Evelyn, M. P.; Hamza, A. V.; Gdowski, G. E.; Madix, R. J. Dynamics of the dissociative adsorption of CO_2 on Ni(100). *Surf. Sci.* **1986**, *167*, 451-473.
(51) Freund, H. J.; Roberts, M. W. Surface chemistry of carbon dioxide. *Surf. Sci. Rep.* **1996**, *25*, 225-273.
(52) Burghaus, U. Surface chemistry of CO_2 – Adsorption of carbon dioxide on clean surfaces at ultrahigh vacuum. *Prog. Surf. Sci.* **2014**, *89*, 161-217.
(53) Neugebohren, J.; Borodin, D.; Hahn, H. W.; Altschäffel, J.; Kandratsenka, A.; Auerbach, D. J.; Campbell, C. T.; Schwarzer, D.; Harding, D. J.; Wodtke, A. M.; Kitsopoulos, T. N. Velocity-resolved kinetics of site-specific carbon monoxide oxidation on platinum surfaces. *Nature* **2018**, *558*, 280-283.
(54) Zhou, L.; Kandratsenka, A.; Campbell, C. T.; Wodtke, A. M.; Guo, H. Origin of thermal and hyperthermal CO_2 from CO oxidation on Pt surfaces: The role of post-transition-state dynamics, active sites, and chemisorbed CO_2. *Angew. Chem. Int. Ed.* **2019**, *58*, 6916-6920.

Table 1. SVP values for CO_2 dissociation on the Cu(110) surface at the two transition states.

Mode	SVP	
	TS1	TS2
v_{as}	0.081	0.684
v_{ss}	0.074	0.565
v_{b}	0.274	0.241
x	0.105	0.296
y	0.005	0.003
z	0.825	0.088

Table 2. Averaged characteristic times for reaction and scattering trajectories, including those for dissociation (T_{diss}), scattering (T_{scat}), passing TS1 (T_{TS1}), between TS1 and TS2 ($T_{TS1\text{-}TS2}$) for dissociative trajectories, and between TS1 and TS1 ($T_{TS1\text{-}TS1}$) for scattered trajectories.

	Translational energy (eV)	T_{diss} (fs)	T_{scat} (fs)	T_{TS1} (fs)	$T_{TS1\text{-}TS2}$ (fs)	$T_{TS1\text{-}TS1}$ (fs)
v=0	1.7	754	1162	204	491	957
	2.0	629	1150	189	369	960
v_{as}=1	1.7	731	1326	204	443	1121
	2	585	1314	188	368	1124
v_{ss}=1	1.7	692	1193	206	415	989
	2.0	573	1163	189	314	973
v_b=2	1.7	666	1224	203	385	1020
	2.0	605	1261	188	358	1071

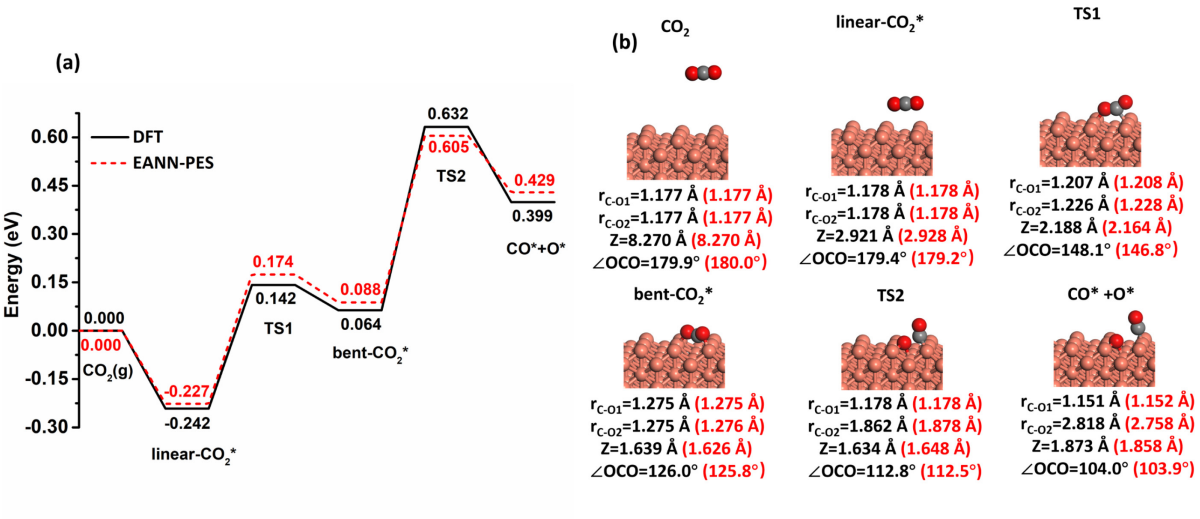

Figure 1. Comparison of (a) energies (in eV) and (b) geometries of adsorption minima, transition states and dissociative products along the MEP of CO_2 dissociative chemisorption on the relaxed Cu (110) surface optimized with DFT (black) and with the EANN PES (red).

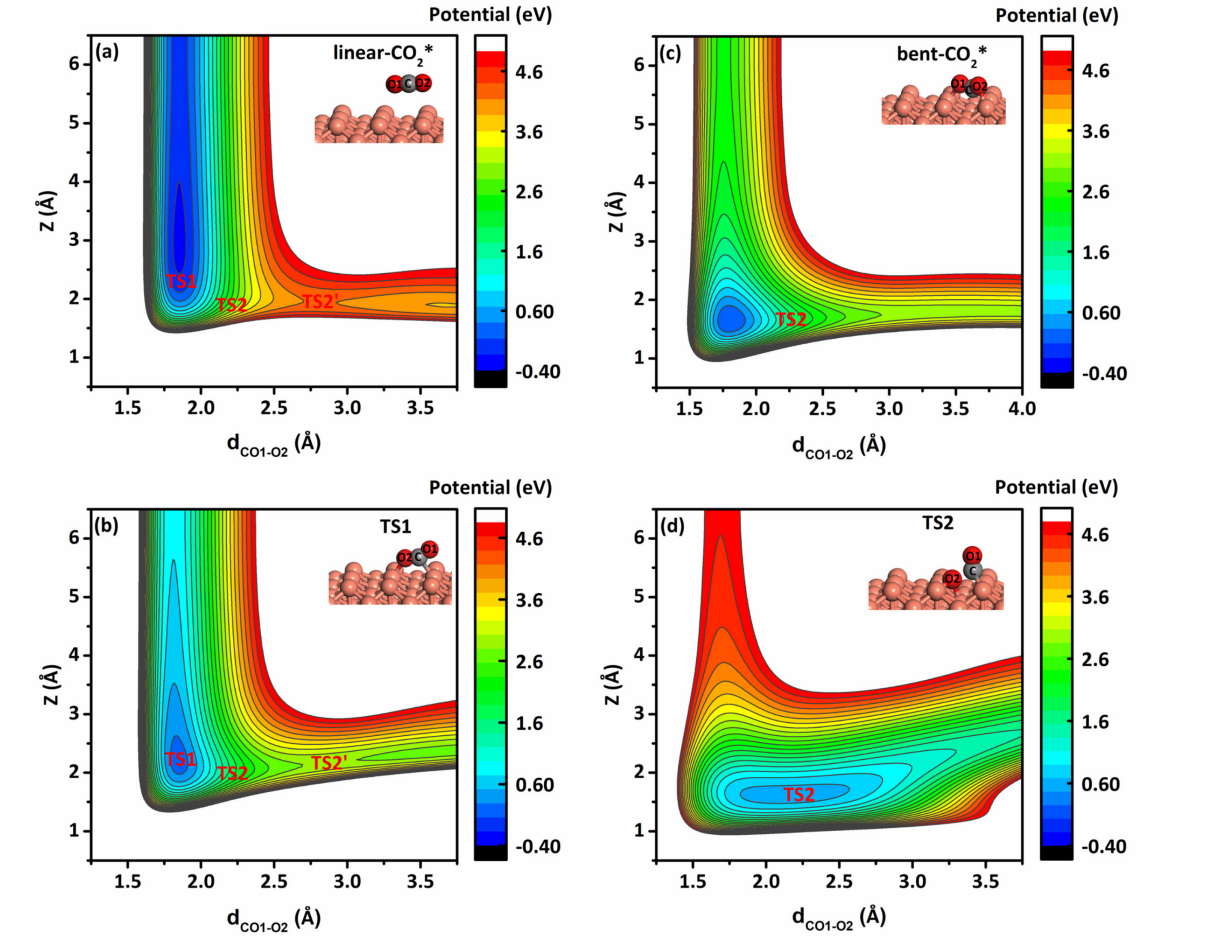

Figure 2. Two-dimensional contours of the EANN PES as a function of the O1C−O2 distance (d_{CO1-O2}) and the molecular height (Z) above the surface, with other coordinates of CO_2 and substrate Cu atoms are fixed at the geometry of (a) linear-CO_2*, (b) TS1, (c) bent-CO_2* and (d) TS2, respectively. The red labels in the contour plots indicate the Z and O1C−O2 distances of the corresponding saddle point. TS2′ is a local saddle point, but its geometric character is close to that of TS2.

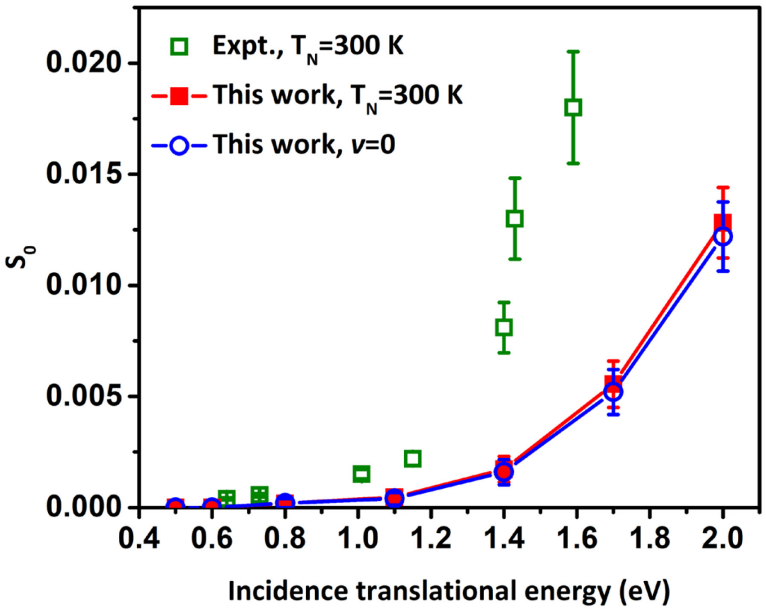

Figure 3. Calculated normal incident dissociative sticking probabilities (S_0) as a function of incidence translational energy, compared with the experimental data at T_N=300 K.[14]

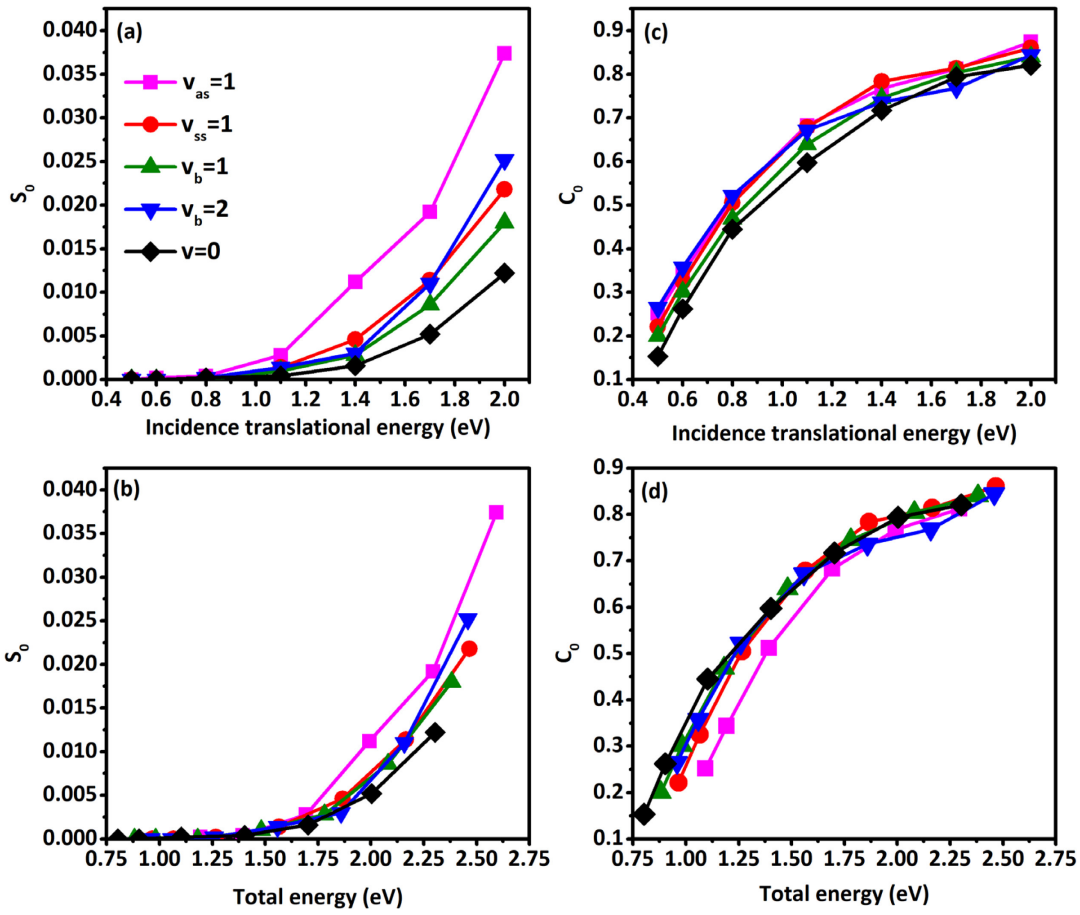

Figure 4. Calculated normal incident dissociative sticking probabilities (S_0) as a function of the incidence translational energy (a) and total energy (b) for several CO_2 vibrational states. The total energy equals to the sum of the translational, rotational, and vibrational energy of the impinging CO_2. For comparison, the capture probabilities (C_0) are shown as a functional of incidence translational energy (c) and total energy (d). The vibrational energies of v=0, v_b=1, v_b=2, v_{ss}=1, v_{as}=1 states are 0.304, 0.381, 0.459, 0.466, and 0.593 eV, respectively, relative to the CO_2 potential minimum.

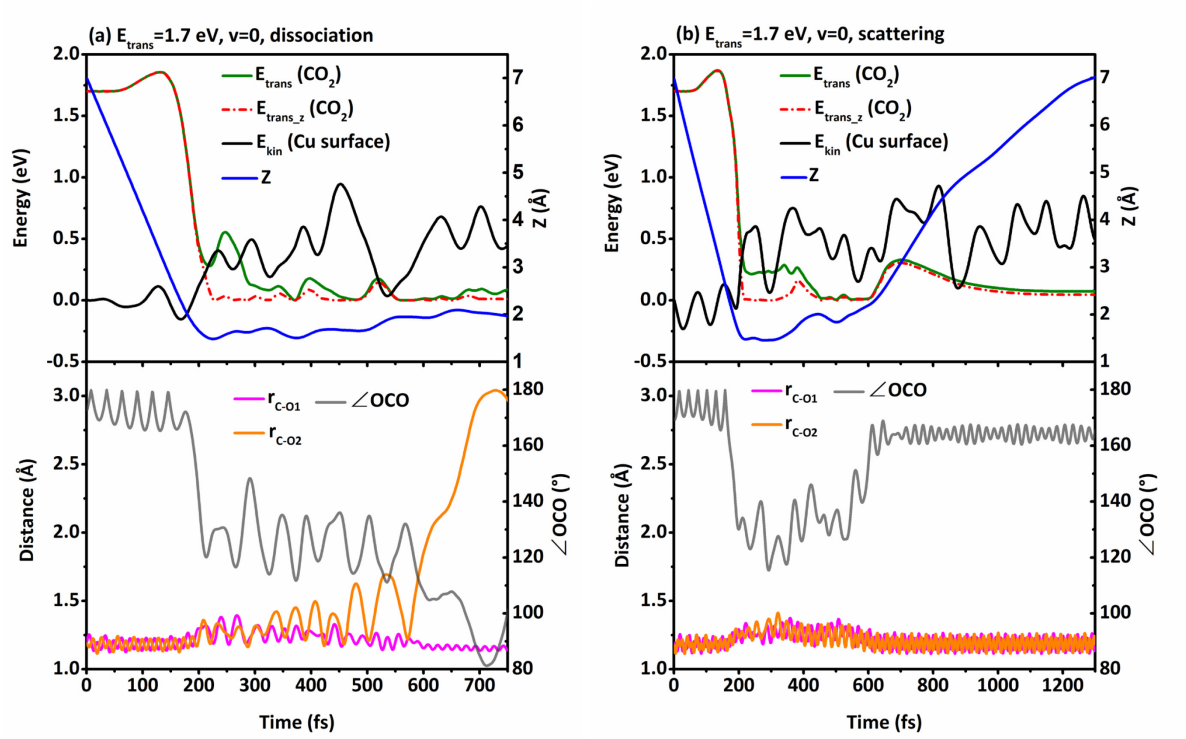

Figure 5. Time evolution of energetic and geometric parameters for two representative trajectories for dissociation (a) and scattering (b) from the Cu(110) surface starting with CO_2(v=0) at the incidence kinetic energy of 1.7 eV. The energetic parameters include the translational energy of CO_2 (E_{trans}) along the surface normal (E_{trans_z}) and the kinetic energy of all Cu atoms (E_{kin}). The geometric parameters include the two C-O bond lengths ($r_{C\text{-}O1}$ and $r_{C\text{-}O2}$), the height (Z) of the CO_2 COM and the OCO bond angle ($\angle$OCO).

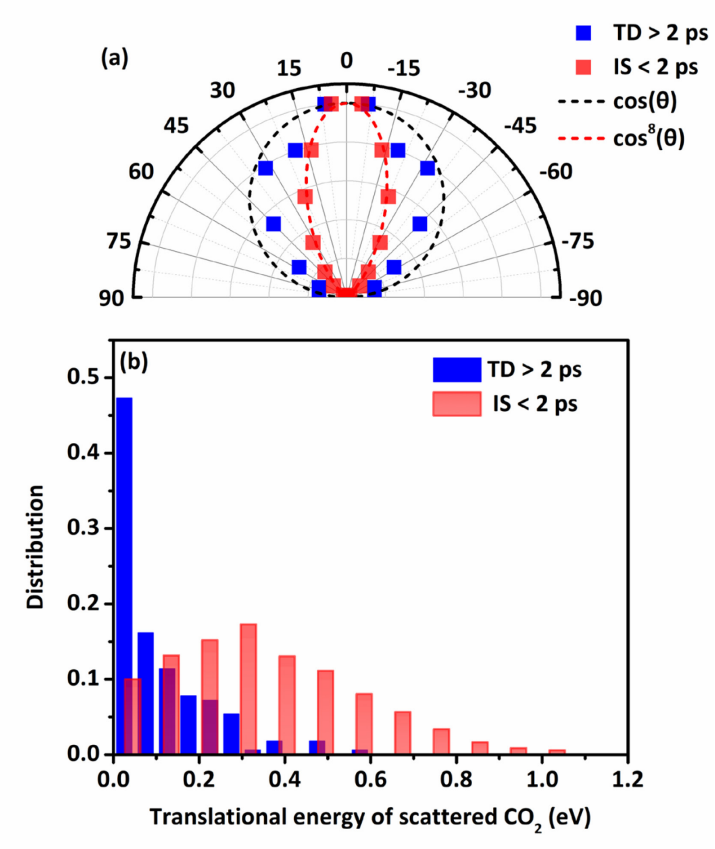

Figure 6. Calculated (a) angular distribution and (b) translational energy distribution for scattered CO_2 from Cu (110) surface with TD (T_{scatt} > 2 ps) and IS (T_{scatt} < 2 ps) trajectories.

TOC graphic

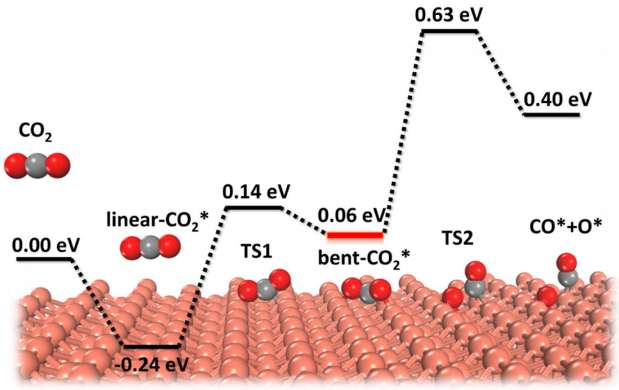
0.63 eV
0.40 eV
CO2
0.14 eV
linear-CO2*
0.06 eV
0.00 eV
TS1
bent-CO2*
TS2
CO*+O*
-0.24 eV